A Deep Learning-Based Approach to Resource Allocation in UAV-aided Wireless Powered MEC Networks

Wanmei Feng*, Jie Tang*, Nan Zhao†, Xiuyin Zhang*, Xianbin Wang‡, Kai-Kit Wong§

*School of Electronic and Information Engineering, South China University of Technology, Guangzhou, China
†Faculty of Electronic Information and Electrical Engineering, Dalian University of Technology, Dalian, China
‡Department of Electrical and Computer Engineering, Western University, London, Ontario N6A5B9, Canada
§Department of Electronic and Electrical Engineering, University College London, WC1E 6BT London, U.K.

Abstract—Beamforming and non-orthogonal multiple access (NOMA) are two key techniques for achieving spectral efficient communication in the fifth generation and beyond wireless networks. In this paper, we jointly apply a hybrid beamforming and NOMA techniques to an unmanned aerial vehicle (UAV)-carried wireless-powered mobile edge computing (MEC) system, within which the UAV is mounted with a wireless power charger and the MEC platform delivers energy and computing services to Internet of Things (IoT) devices. We aim to maximize the sum computation rate at all IoT devices whilst satisfying the constraint of energy harvesting and coverage. The considered optimization problem is non-convex involving joint optimization of the UAV's 3D placement and hybrid beamforming matrices as well as computation resource allocation in partial offloading pattern, and thus is quite difficult to tackle directly. By applying the polyhedral annexation method and the deep deterministic policy gradient (DDPG) algorithm, we propose an effective algorithm to derive the closed-form solution for the optimal 3D deployment of the UAV, and find the solution for the hybrid beamformer. A resource allocation algorithm for partial offloading pattern is thereby proposed. Simulation results demonstrate that our designed algorithm yields a significant computation performance enhancement as compared to the benchmark schemes.

Index Terms—Hybrid beamforming, mobile edge computing, non-orthogonal multiple access, unmanned aerial vehicle

I. INTRODUCTION

THE development of the Internet-of-Things (IoT) applications has fuelled an exponential growth of IoT devices, which are widely deployed to support diverse smart applications [1]. However, many of these intelligent applications are computationally-intensive and latency-sensitive, which are extremely difficult for IoT devices to handle due to their limited computing capacity. Mobile edge computing (MEC) can potentially be a very effective technique for enhancing the computing capacity of IoT devices through offloading. With MEC, the IoT devices can offload partial or entire computation missions to the computing servers that are located at the network edge, namely the base stations (BSs) [2].

Recently, non-orthogonal multiple access (NOMA) has been viewed as an emerging technique for the fifth generation (5G) and beyond 5G (B5G) wireless networks [3]. It has been proved that combining MEC and NOMA can reduce the latency and energy cost, and therefore improve the performance of computation offloading in the MEC paradigms. Nevertheless, when the IoT devices are deployed in an area where communication

facilities are sparsely distributed, it is not efficient for MEC servers to offer computing services.

Unmanned aerial vehicles (UAVs) and the wireless power transfer (WPT) serve as two potential solutions to extend the battery-life of IoT devices in geographically constrained areas. Therefore, the integration of MEC and UAVs as well as WPT can improve the computing capacity of IoT devices due to the shorten of the transmission distance and the extension of MEC service time. In fact, although the computation performance of IoT devices can be enhanced by WPT, the performance gain is very limited due to the severe path loss. To address this problem, energy beamforming is used to focus the transmitted energy on the receivers. However, few works have applied the beamforming technique within wireless-powered MEC networks.

In this paper, we investigate the the sum computation rate maximization problem in a UAV-aided wireless-powered MEC network, where the UAV's 3D placement and the hybrid beamforming matrices as well as computation resource allocation are jointly optimized. To tackle this problem, we first design the sequential unconstrained convex minimization (SUCM) based placement optimization algorithm to achieve the optimal 3D placement of the UAV. After that, a learning-based two stage hybrid beamforming scheme is designed for optimizing the hybrid beamforming matrices. Inspired by the alternative optimization method and Lagrange dual method, we finally develop an effective resource allocation scheme to optimize the computation resource allocation.

II. SYSTEM MODEL AND PROBLEM FORMULATION

A. System Model

As depicted in Fig. 1, we consider a UAV-aided wireless powered MEC system with a UAV and K IoT devices, where an $M \times N$ rectangular antenna array is installed on the UAV and all IoT devices have single antenna. In particular, the UAV is setup with a radio frequency (RF) energy transmitter and a communication unit as well as an MEC server, while each device is setup with an energy harvesting unit, a communication unit as well as a computation unit [2].

We assume that all devices need to perform a certain computing task during a given period T. A harvest-then-offload protocol is adopted, in which the whole period T contains three phases. In the first phase with duration aT ($a \in [0, 1]$), the
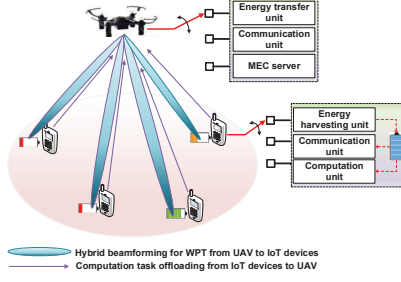
Fig. 1: Illustration of a multiuser UAV-aided wireless powered MEC system with hybrid beamforming.

UAV forms multi-beams to broadcast wireless energy to all IoT devices. Subsequently, IoT devices offload the computation tasks to the UAV platform in the second phase with time duration $(1-a)T$. After receiving the offloaded tasks, the UAV computes and replies to the corresponding devices during the third phase. Since the computing capacity of the UAV is much greater than the IoT devices, the computation and downloading time for the UAV is neglected [2].

In general, the horizontal location of the UAV is denoted as $z_u = (x_u, y_u)$, with its altitude as h_u. The position of the device k on the ground is denoted as $z_k = (x_k, y_k)$, where $k \in \mathcal{M} = \{1, 2, \cdots K\}$. The channel between the UAV and device k is represented by [4]

$$\mathbf{h}_k = \sqrt{\beta_0 d_k^{-\alpha}} \mathbf{a}(\theta, \phi), \tag{1}$$

where α ($\alpha \geq 2$) and $d_k = \sqrt{(x_k - x_u)^2 + (y_k - y_u)^2 + h_u^2}$ are the path loss exponent and the distance between the UAV and the device k, respectively. Also, β_0 indicates the channel power gain at the reference distance of $d_0 = 1$ m. Let the wavelength and the array spacing between antenna elements be denoted by λ and d_{array}. The steering vector $\mathbf{a}(\theta, \phi)$ of an $M \times N$ antenna array is represented by [4]

$$\begin{aligned} \mathbf{a}(\theta, \phi) = &[1, \cdots, e^{j2\pi/\lambda d_{array} \sin(\theta)[(m-1)\cos(\phi)+(n-1)\sin(\phi)]}, \\ &\cdots, e^{j2\pi/\lambda d_{array} \sin(\theta)[(M-1)\cos(\phi)+(N-1)\sin(\phi)]}]^T, \end{aligned} \tag{2}$$

where (θ, ϕ) denotes the steering angles.

We consider a hybrid beamforming structure for energy beamforming at the UAV, which includes an analog beamformer and a digital beamformer. The antenna array is partitioned into several sub-arrays, wherein each RF chain is connected to a sub-array and the number of antenna elements per sub-array is N_a^t. We assume that the total number of RF chains in the hybrid beamforming architecture is equal to the number of IoT devices, i.e, $N_{RF} = K$. The total number of antenna elements can be obtained by $M \cdot N = N_{RF} \cdot N_a^t$. Then, the channel power gain from the UAV to the device k is written as

$$|\mathbf{h}_k^H \mathbf{F} \mathbf{w}_k|^2 = \frac{\beta_0}{[(x_k - x_u)^2 + (y_k - y_u)^2 + h^2]^{\alpha/2}} |\mathbf{B}_k|^2, \tag{3}$$

where $\mathbf{B}_k = \mathbf{a}^H(\theta, \phi)\mathbf{F}\mathbf{w}_k$ and $\mathbf{W} = [\mathbf{w}_1, \mathbf{w}_2, \cdots, \mathbf{w}_K]^T$ represents the $N_{RF} \times K$ digital beamforming matrix. $\mathbf{F}$ denotes the analog beamforming matrix given by

$$\begin{bmatrix} \mathbf{a}(\theta_1, \phi_1) & \mathbf{0}_{N_a^t} & \cdots & \mathbf{0}_{N_a^t} \\ \mathbf{0}_{N_a^t} & \mathbf{a}(\theta_2, \phi_2) & \cdots & \mathbf{0}_{N_a^t} \\ \vdots & \vdots & \ddots & \vdots \\ \mathbf{0}_{N_a^t} & \mathbf{0}_{N_a^t} & \cdots & \mathbf{a}(\theta_{N_{RF}}, \phi_{N_{RF}}) \end{bmatrix}. \tag{4}$$

The diagonal entry $\mathbf{f}_i = \mathbf{a}(\theta_i, \phi_i)$ indicates the analog steering vector for the ith sub-array, $i \in \{1, 2, \cdots, N_{RF}\}$, and (θ_i, ϕ_i)

corresponds to the designed steering angles.

The harvested energy at device k is expressed as

$$E_k = \tau_0 \xi_0 P_0 |\mathbf{h}_k^H \mathbf{F} \mathbf{w}_k|^2, \tag{5}$$

where P_0 denotes the transmit power of the UAV and τ_0 indicates the energy harvesting time. $\xi_0 (0 < \xi_0 < 1)$ represents the energy conversion efficiency.

B. Partial Offloading

1) Local Computing: Let the number of computation cycles required for computing one bit of raw data be denoted by C. We define the CPU frequency of device k as f_k, which holds $f_k \leq f_{max}$. The computation rate of device k is given by

$$r_{L,k}^{Par} = \frac{f_k t_k}{CT}, \ k \in \mathcal{M}, \tag{6}$$

where $0 < t_k < T$ represents the computation time of the kth device. The consumed energy at device k is written as

$$E_{L,k}^{Par} = \tau_k f_k^3 t_k, \ k \in \mathcal{M}, \tag{7}$$

where τ_k indicates the effective capacitance coefficient.

2) Offloading Computation: We exploit the NOMA scheme that enables all the IoT devices to send tasks to the UAV simultaneously. The channel power gain from the kth device to the UAV is expressed as

$$g_k = \frac{\beta_0}{[(x_k - x_u)^2 + (y_k - y_u)^2 + h_u^2]^{\alpha/2}}. \tag{8}$$

The channel power gains between IoT devices and the UAV are ranked in an ascending order $g_1 < g_2 < \cdots < g_K$. Let B and P_k be the communication bandwidth and the transmit power of the kth device. The total computation rate of device k under a given period $(1-a)T$ is given by

$$r_{o,k}^{Par} = \begin{cases} \frac{f_k t_k}{CT} + B(1-a)\log_2\left(1 + \frac{P_k g_k}{\sum_{i=k+1}^{K} P_i g_i + N_0}\right), \\ \qquad\qquad\qquad 1 \leq k \leq K-1, \\ \frac{f_k t_k}{CT} + B(1-a)\log_2\left(1 + \frac{P_k g_k}{N_0}\right), k = K, \end{cases} \tag{9}$$

where N_0 denotes the receiver noise power. The energy harvesting constraints are written as

$$\tau_k f_k^3 t_k + P_k(1-a)T \leq aT\xi_0 P_0 |\mathbf{h}_k^H \mathbf{F} \mathbf{w}_k|^2, k \in \mathcal{M}, \tag{10}$$

$$aT\xi_0 P_0 |\mathbf{h}_k^H \mathbf{F} \mathbf{w}_k|^2 \leq T\xi_0 P_0 |\mathbf{h}_k^H \mathbf{F} \mathbf{w}_k|^2 \leq \tau_k f_{max}^3 T, k \in \mathcal{M}. \tag{11}$$

C. Problem Formulation

The sum computation rate maximization problem is written as

$$\begin{aligned} \text{(P1)} : \max_{\substack{x_u, y_u, h_u, \mathbf{W}, \mathbf{F}, \\ a, P_k, t_k, f_k}} \quad \sum_{k \in \mathcal{M}} &\left[\frac{f_k t_k}{CT} \right. \\ &\left. + B(1-a)\log_2\left(1 + \frac{P_k g_k}{\sum_{i=k+1}^{K} P_i g_i + N_0}\right) \right] \end{aligned} \tag{12a}$$

$$\text{s.t.} \ \tau_k f_k^3 t_k + P_k(1-a)T \leq aT\xi_0 P_0 |\mathbf{h}_k^H \mathbf{F} \mathbf{w}_k|^2, \tag{12b}$$

$$\|z_k - z_u\|^2 \leq h_u^2 \tan^2 \Theta, \tag{12c}$$

$$h_{min} \leq h_u \leq h_{max}, \tag{12d}$$

$$0 \leq t_k \leq T, \tag{12e}$$

$$0 \leq a \leq 1, \tag{12f}$$

$$P_k \geq 0, \tag{12g}$$

$$0 \leq f_k \leq f_{max}. \tag{12h}$$

Constraint (12b) represents the energy harvesting constraint for all the IoT devices. Constraint (12c) is the area coverage

constraint, where 2Θ denotes the effective illumination angle [4]. Constraint (12d) is the boundary constraint for the UAV's flight altitude. Constraint (12e) guarantees that the computation time for IoT devices is no longer than the whole period T. Constraint (12f) corresponds to the time constraint for WPT. Constraints (12g) and (12h) denote the computation offloading power constraint and the CPU frequency constraint, respectively. Problem (P1) is a mixed combinatorial non-convex optimization problem due to the coupling variables. To address this problem, we decouple the considered problem into two subproblems, where the solutions are obtained through two steps. In the first step, the 3D placement of the UAV and the hybrid beamforming matrices are optimized first for maximizing the harvested energy at the IoT devices. Then, a resource allocation algorithm is designed to maximize the sum computation rate at the IoT devices.

III. 3D PLACEMENT FOR UAV AND HYBRID BEAMFORMING FOR WPT

A. Optimal UAV 3D Placement

To optimize the 3D location of the UAV, we investigate the following energy harvesting maximization problem:

$$(P2): \max_{\substack{x_u,y_u,h_u, \\ \mathbf{W},\mathbf{F}}} \sum_{k=1}^{K} aT\xi_0 P_0 |\mathbf{h}_k^H \mathbf{F}\mathbf{w}_k|^2 \tag{13a}$$

$$\text{s.t. } \|z_k - z_u\|^2 \le h_u^2 \tan^2\Theta, \tag{13b}$$

$$h_{min} \le h_u \le h_{max}, \tag{13c}$$

$$\sum_{k=1}^{K} \| \mathbf{F}\mathbf{w}_k \|^2 \le P_{th}, \tag{13d}$$

where P_{th} is the total transmit power budget. For given $\mathbf{W}$ and $\mathbf{F}$, problem (P2) is non-convex. Thus, we first solve (x_u, y_u) with fixed h_u. With $A_k = aT\xi_0 P_0 \beta_0 |\mathbf{B}_k|^2$, $\zeta_k(x_u, y_u) = (x_k - x_u)^2 + (y_k - y_u)^2 + h_u^2$ and $\eta_k(\zeta_k(x_u, y_u)) = A_k[\zeta_k(x_u, y_u)]^{-\alpha/2}$, problem (P2) is formulated as

$$(P2.1): \max_{x_u,y_u} \sum_{k}^{K} \eta_k(\zeta_k(x_u, y_u)), \tag{14}$$

where $\zeta_k(x_u, y_u)$ is convex over (x_u, y_u) and $\eta(\cdot)$ is a strictly convex function and strictly decreasing on $\mathbf{R}^+$. Since $\lim_{x_u,y_u \to \infty} \zeta_k(x_u, y_u) = +\infty$ and $\lim_{\zeta_k(x_u,y_u) \to \infty} \eta_k(\zeta_k(x_u, y_u)) = 0$, problem (P2.1) is neither a convex nor concave optimization problem [4], [5]. Therefore, we develop a SUCM-based placement optimization algorithm to tackle problem (P2.1).

We convert problem (P2.1) into problem (P2.2) by using an auxiliary variable $\mathbf{z} = [z_1, z_2, \cdots, z_K]^T$

$$(P2.2): \max_{x_u,y_u,\mathbf{z}} \sum_{k=1}^{K} \eta_k(z_k) \tag{15a}$$

$$\text{s.t. } \zeta_k(x_u, y_u) \le z_k, \ k = 1, 2, \cdots, K. \tag{15b}$$

Denote

$$\mathcal{D} = \{\mathbf{z} \in \mathbf{R}_+^k : \zeta_k(x_u, y_u) \le z_k, \ k = 1, 2, \cdots, K, \\ \exists (x_u, y_u) \in \mathbf{R}^2\}. \tag{16}$$

From (16), problem (P2.2) can be equivalently written as

$$(P2.3): \max_{\mathbf{z} \in \mathcal{D}} \eta(\mathbf{Z}), \tag{17}$$

where $\eta(\mathbf{z}) = \sum_{k=1}^{K} \eta_k(z_k)$. Since $\eta(\mathbf{z})$ is a convex function and $\mathcal{D}$ represents a compact convex set, problem (P2.3) is a convex maximization problem.

Denote $\mathcal{C} = \{\mathbf{z} \in \mathbf{R}_+^k : \eta(\mathbf{z}) \le \eta(\mathbf{z}^*)\}$, $\widetilde{\mathcal{C}} = \{\mathbf{z} - \mathbf{z}_0 \mid \mathbf{z} \in \mathcal{C}\}$ and $\widetilde{\mathcal{D}} = \{\mathbf{z} - \mathbf{z}_0 \mid \mathbf{z} \in \mathcal{D}\}$. Here, $\mathbf{z}_0 = [z_{0,1}, z_{0,2}, \cdots, z_{0,K}]^T$ represents a feasible point, and $\mathbf{z}^*$ is the best feasible solution. Note that the solutions in $\mathcal{C}$ and $\widetilde{\mathcal{C}}$ are not better than $\mathbf{z}^*$. If $\widetilde{\mathcal{D}} \subset \widetilde{\mathcal{C}}$, it follows that $\mathbf{z}^*$ is the best solution; otherwise, it follows that $\mathbf{z}^*$ is a local solution. By using the concept of polar set [6], we have the following proposition to determine whether $\widetilde{\mathcal{D}} \subset \widetilde{\mathcal{C}}$.

Proposition 1: Let $\mathcal{V}$ denote the vertex set of the polytope $\mathcal{B}$. $\widetilde{\mathcal{C}}^{\mathrm{o}} \subset \widetilde{\mathcal{D}}^{\mathrm{o}}$ satisfies

$$\max_{\mathbf{z} \in \mathcal{D}} \mathbf{v}^T \mathbf{z} \le 1, \ \forall \mathbf{v} \in \mathcal{V}, \tag{18}$$

where $\mathbf{v} = [v_1, v_2, \cdots, v_K]^T$. $\widetilde{\mathcal{C}}^{\mathrm{o}}$ and $\widetilde{\mathcal{D}}^{\mathrm{o}}$ denote the polar set of $\widetilde{\mathcal{C}}$ and $\widetilde{\mathcal{D}}$. The polytope $\mathcal{B}$ holds $\widetilde{\mathcal{C}}^{\mathrm{o}} \subset \mathcal{B} \subset \mathbf{R}_-^K$ [5].

Proof: The proof of Proposition 1 is omitted here. ∎

We use Proposition 1 and let $-\mathbf{v} = \mathbf{w} = [w_1, w_2, \cdots, w_K]^T$. Next, consider problem (P2.2) in (15) and notice that $\widetilde{\mathcal{D}} = \{\mathbf{z} - \mathbf{z}_0 \mid \mathbf{z} \in \mathcal{D}\}$, then (x_u^*, y_u^*) can be obtained by dealing with the equivalent problem derived from (18) as

$$\min_{x_u,y_u} \sum_{k=1}^{K} w_k[\zeta_k(x_u, y_u) - z_{0,k}]. \tag{19}$$

By discarding the constant term $-\mathbf{w}^T \mathbf{z}_0$, (19) is written as

$$\min_{x_u,y_u} \sum_{k=1}^{K} w_k \left[(x_k - x_u)^2 + (y_k - y_u)^2 + h_u^2 \right]. \tag{20}$$

Thus, the closed-form expression of (x_u^*, y_u^*) from the above problem is expressed as

$$x_u^* = \frac{\sum_{k=1}^{K} w_k x_k}{\sum_{k=1}^{K} w_k}, \ \ y_u^* = \frac{\sum_{k=1}^{K} w_k y_k}{\sum_{k=1}^{K} w_k}. \tag{21}$$

According to [5], the optimal solution of problem (P2.3) can be produced by the polyhedral annexation procedure. In particular, we first initiate a polytope $\mathcal{B}^{(1)}$ with the vertex set $\mathcal{V}^{(1)} = \{\mathbf{v}^{(1)}\}$ that is represented by $\mathcal{B}^{(1)} = \left\{ \mathbf{z} \in \mathbf{R}_-^K : -\sum_{k=1}^{K} z_k \le \frac{1}{\varsigma} \right\}$. The best feasible solution $\mathbf{z}^*$ holds $\eta(\mathbf{z}_0) \le \eta(\mathbf{z}^*)$. Here, ς is small enough such that $\varsigma > 0$ holds, and m denotes the iteration index. Based on the vertex set $\mathcal{V}^{(m)}$, we calculate $-\psi(\mathbf{w})$ and (x_u^*, y_u^*) by dealing with the problem in (20), where $\psi(\mathbf{w})$ is the objection function value of (20). Here, if the optimal value of $\mathbf{w}$ satisfies $\max_{-\mathbf{w} \in \mathcal{V}^{(m)}} -\psi(\mathbf{w}) + \mathbf{w}^T \mathbf{z}_0 \le 1$, it follows that $\mathbf{z}^*$ is a globally optimal solution; otherwise, it follows that $\mathbf{z}^*$ is a local optimum. Then, we use the analytic center cutting plane method (ACCPM) to avoid the local solutions. Specifically, we calculate $\overline{w}$ and $\overline{z}$ by $\overline{w} \in \max_{-\mathbf{w} \in \mathcal{V}^{(m)}} -\psi(\mathbf{w}) + \mathbf{w}^T \mathbf{z}_0$ and $\overline{z}_k = \zeta_k(\overline{x}_u, \overline{y}_u)$, respectively. Here, $\overline{x}_u = \frac{\sum_{k=1}^{K} \overline{w}_k x_k}{\sum_{k=1}^{K} \overline{w}_k}$ and $\overline{y}_u = \frac{\sum_{k=1}^{K} \overline{w}_k y_k}{\sum_{k=1}^{K} \overline{w}_k}$. If $\eta(\overline{z}) > \eta(\mathbf{z}^*)$, we update $\mathbf{z}^*$ by $\overline{z}$. On the other hand, if $\eta(\overline{z}) \le \eta(\mathbf{z}^*)$, we generate the cutting planes ε and update the polytope $\mathcal{B}^{(m+1)}$ by computing $\varepsilon = \sup\{\rho : \eta(\mathbf{z}_0 + \rho(\overline{z} - \mathbf{z}_0)) \le \eta(\mathbf{z}^*)\}$ and $\mathcal{B}^{(m+1)} = \mathcal{B}^{(m)} \cap \left\{ \mathbf{z} : \mathbf{z}^T(\overline{z} - \mathbf{z}_0) \le \frac{1}{\varepsilon} \right\}$. Similarly, we repeat the above procedure to build a sequential nested polytope for which $\mathcal{B}^{(1)} \supset \mathcal{B}^{(2)} \supset \cdots \supset \mathcal{B}^{(m)} \supset \widetilde{\mathcal{C}}^{\mathrm{o}}$.

With the solved (x_u^*, y_u^*), it can be confirmed that (13a) is monotonic decreasing in h_u. From (13b), it follows that the optimal flight altitude h_u^* is expressed as

$$h_u^* = \max \left\{ \frac{\sqrt{Q_{\max}}}{\tan\Theta}, h_{min} \right\}, \tag{22}$$

where $Q_{\max} = \max_{k=1,\cdots,K} \| z_k - z_u \|^2$.

B. MOEA/D Based Analog Beamformer Design

The analog beamformer is designed by optimizing the side-lobe level (SLL), array gain and beamwidth through controlling the phases [4]. Mathematically, this can be solved by a multi-objective optimization framework

$$\min \ F(\boldsymbol{\vartheta}) = (f_1(\boldsymbol{\vartheta}), f_2(\boldsymbol{\vartheta}), f_3(\boldsymbol{\vartheta}))^T$$
$$\text{s.t. } \boldsymbol{\vartheta} \in \mathbf{R}^{M \times N}, \tag{23}$$

where $f_1(\boldsymbol{\vartheta}) = SLL(\boldsymbol{\vartheta})$, $f_2(\boldsymbol{\vartheta}) = \frac{1}{|\mathbf{E}(\theta,\phi)|}$, and $f_3(\boldsymbol{\vartheta}) = \frac{1}{|\Theta_{h,e}|}$. $\boldsymbol{\vartheta} = [\vartheta_{1n}, \cdots, \vartheta_{mn}, \cdots, \vartheta_{MN}]^T$ represents the phases of the $M \times N$ antenna array. $SLL(\boldsymbol{\vartheta}) = 20 \log \frac{|\text{AF}_{msl}|}{|\text{AF}_{max}|}$ represents the SLL of the $M \times N$ antenna array [7], where AF_{msl} and AF_{max} denote the array factor of the maximum SLL and the main-lobe, respectively [4]. The array factor of the $M \times N$ antenna array is $\text{AF} = \sum_{m=1}^{M} \sum_{n=1}^{N} I_{mn} \times e^{j2\pi/\lambda d_{array} \sin(\theta)[(m-1)\cos(\phi)+(n-1)\sin(\phi)]+\vartheta_{mn}}$ [7]. $\mathbf{E}(\theta,\phi) = \mathbf{a}^H(\theta,\phi)\mathbf{F}$ denotes the synthesized pattern, and $\mathbf{F} = e^{j\boldsymbol{\vartheta}}$. $\Theta_{h,e}$ indicates the elevation plane half-power beamwidth. To solve problem (23), a multiobjective evolutionary algorithm (MOEA/D) solution is developed here. This algorithm consists of the following steps:

- *Input*: Let $\{N_{sub}, \boldsymbol{\beta}^i, S_{nei}, iter\}$ be a set of input parameters. Here, N_{sub} represents the number of subproblems. $\boldsymbol{\beta}^i = (\beta_1^i, \cdots, \beta_d^i)^T, i = 1, \cdots, N_{sub}, 1 \le d \le 3$ denotes the weight vector of the ith subproblem. S_{nei} indicates the number of weight vectors considered to be neighbors of each weight vector and $iter$ is the iteration index.
- *Output*: The output is a non-dominated set ND.
- *Initialization*: We first choose S_{nei} as the closest weight vectors of $\boldsymbol{\beta}^i$ by computing the Euclidean distance, whose indices are stored in $\mathcal{C}(i)$. Then, we produce $\boldsymbol{\vartheta}_1, \cdots, \boldsymbol{\vartheta}_{N_{sub}}$ randomly, and then update the F-values $FV_i = F(\boldsymbol{\vartheta}_i)$ and the best-so-far solutions $\mathcal{L} = (L_1, \cdots, L_j, \cdots, L_d)^T$. Here, $L_j = \min\{f_j(\boldsymbol{\vartheta}), \boldsymbol{\vartheta} \in \mathbf{R}^{M \times N}\}$.
- *Update*: For each $i = 1, \cdots, N_{sub}$, we extract two weight vectors $\boldsymbol{\vartheta}_k$ and $\boldsymbol{\vartheta}_l$ from $\mathcal{C}(i)$ and then obtain a new solution $\boldsymbol{x}$ by exploiting the differential evolution (DE) algorithm. Then, we update the best-so-far solutions and the F-value of $\boldsymbol{\vartheta}_i$. Specifically, for $j = 1, \cdots, d$, if $L_j > f_j(\boldsymbol{x})$, it follows that $L_j = f_j(\boldsymbol{x})$; if $g^{te}(\boldsymbol{x} \mid \boldsymbol{\beta}^j, \mathcal{L}) \le g^{te}(\boldsymbol{\vartheta}_j \mid \boldsymbol{\beta}^j, \mathcal{L})$, it follows that $\boldsymbol{\vartheta}_j = \boldsymbol{x}$ and $FV_j = F(\boldsymbol{x})$. Here, $g^{te}(\boldsymbol{x} \mid \boldsymbol{\beta}^j, \mathcal{L}) = \max_{1 \le t \le d}\{\beta_t^j | f_t(\boldsymbol{x}) - L_t|\}$ [8]. $F(\boldsymbol{x})$ will be stored in ND if it dominates other weight vectors, and all weight vectors from ND dominated by $F(\boldsymbol{x})$ are excluded.
- *Stopping*: The algorithm stops if the iterations have converged; otherwise, go back to *Update*.

C. DDPG Based Digital Beamformer Design

Based on the optimal 3D placement of the UAV and the analog beamformer, problem (P2) is then reformulated as

$$(\text{P2.4}) : \max_{\mathbf{W}} \ \sum_{k=1}^{K} aT\xi_0 P_0 |\mathbf{h}_k^H \mathbf{F} \mathbf{w}_k|^2 \tag{24a}$$

$$\text{s.t. } \sum_{k=1}^{K} \| \mathbf{F}\mathbf{w}_k \|^2 \le P_{th}, \tag{24b}$$

Problem (P2.4) can be converted into a convex semi-definite programming (SDP) problem, and hence can be addressed by the interior-point methods [9]. However, the interior-point methods have high memory requirements. Thus, we apply the deep deterministic policy gradient (DDPG) algorithm to optimize the digital beamformer which can be described as follows:

- *Initialization:* Initialize the critic network $Q(s, a|\theta^Q)$ with weights θ^Q and actor network $\mu(s|\theta^\mu)$ with θ^μ. Initialize the target network Q' with weights $\theta^{Q'}$ and target network μ' with $\theta^{\mu'}$, while $\theta^{Q'} = \theta^Q$ and $\theta^{\mu'} = \theta^\mu$. Initialize the replay memory R.
- *Loop:*
  1) Observe the status s_t. The status includes the distance between the UAV and the IoT devices as well as the unwrapped analog precoding matrix, i.e., $[d_k, real(\mathbf{f}_1), imag(\mathbf{f}_1), \ldots, real(\mathbf{f}_{N_a^t}), imag(\mathbf{f}_{N_a^t})]$.
  2) Generate an action as $a_t = \mu(s_t|\theta^\mu) + \mathcal{N}_t$, where $\mathcal{N}_t$ denotes an exploration process and t is the iteration index. $\mu(s_t|\theta^\mu)$ represents an action generation policy.
  3) Execute action a_t and compute the reward r_t, while observing the next time slot status s_{t+1}. Then, store (s_t, a_t, r_t, s_{t+1}) into the replay memory R.
  4) Randomly choose a training batch of N from R, that is (s_i, a_i, r_i, s_{i+1}), $i \in \{1, \cdots, N\}$. Set $y_i = r_i + \gamma Q'(s_{i+1}, \mu'(s_{i+1}|\theta^{\mu'})|\theta^{Q'})$ and compute the result.
  5) Update the critic network and the actor policy by minimizing the loss $L = \frac{1}{N}\sum_i(y_i - Q(s_i, a_i|\theta^Q))^2$ and the gradient $\Delta_{\theta^\mu}\mathcal{J} \approx \frac{1}{N}\sum_i \Delta_a Q(s, a|\theta^Q)|_{s=s_i, a=\mu(s_i)}\Delta_{\theta|mu}\mu(s|\theta^\mu)|_{s_i}$, respectively. Update the target network weights as $\theta^{Q'} \leftarrow \tau\theta^Q + (1-\tau)\theta^{Q'}$ and $\theta^{\mu'} \leftarrow \tau\theta^\mu + (1-\tau)\theta^{\mu'}$.
- *Stopping:* The algorithm stops if the loop process reaches a predetermined number.
- *Output:* The digital precoding matrix.

IV. NOMA-BASED RESOURCE ALLOCATION ALGORITHM IN PARTIAL OFFLOADING MODE

With solved (x_u^*, y_u^*, h_u^*), $\mathbf{F}^*$ and $\mathbf{W}^*$, problem (P1) is reformulated as

$$(\text{P3}) : \max_{a, P_k, t_k, f_k} \ \sum_{k=1}^{K} \left[\frac{f_k t_k}{CT} \right.$$
$$\left. + B(1-a)\log_2\left(1 + \frac{P_k g_k}{\sum_{i=k+1}^{K} P_i g_i + N_0}\right) \right] \tag{25a}$$

$$\text{s.t. } \tau_k f_k^3 t_k + P_k(1-a)T \le aT\xi_0 P_0 |\mathbf{h}_k^H \mathbf{F}\mathbf{w}_k|^2, \tag{25b}$$
$$0 \le t_k \le T, \tag{25c}$$
$$0 \le a \le 1, \tag{25d}$$
$$P_k \ge 0, \tag{25e}$$
$$0 \le f_k \le f_{max}. \tag{25f}$$

Problem (P3) is non-convex. To solve this problem, the considered problem is decomposed into two subproblems. Particularly, for given a and t_k, problem (P3) is expressed as

$$(\text{P3.1}) : \max_{P_k, f_k} \ \sum_{k=1}^{K} \left[\frac{f_k t_k}{CT} \right.$$
$$\left. + B(1-a)\log_2\left(1 + \frac{P_k g_k}{\sum_{i=k+1}^{K} P_i g_i + N_0}\right) \right] \tag{26a}$$

$$\text{s.t. } \tau_k f_k^3 t_k + P_k(1-a)T \le aT\xi_0 P_0|\mathbf{h}_k^H\mathbf{F}\mathbf{w}_k|^2, \quad (26b)$$

$$P_k \ge 0, \quad (26c)$$

$$0 \le f_k \le f_{max}. \quad (26d)$$

Problem (3.1) is still a non-convex problem due to the second term of (26a). By performing the logarithmic transformation, we transform $\sum_{k=1}^K B(1-a)\log_2\left(1 + \frac{P_k g_k}{\sum_{i=k+1}^K P_i g_i + N_0}\right)$ as

$$B(1-a)\log_2\left(\frac{\sum_{i=1}^K P_i g_i + N_0}{N_0}\right). \quad (27)$$

Using (27), (P3.1) is represented as the following problem

$$(P3.2): \max_{P_k, f_k} \sum_{k=1}^K \frac{f_k t_k}{CT}$$

$$+ B(1-a)\log_2\left(\frac{\sum_{i=1}^K P_i g_i + N_0}{N_0}\right) \quad (28a)$$

$$\text{s.t. } \tau_k f_k^3 t_k + P_k(1-a)T \le aT\xi_0 P_0|\mathbf{h}_k^H\mathbf{F}\mathbf{w}_k|^2, \quad (28b)$$

$$P_k \ge 0, \quad (28c)$$

$$0 \le f_k \le f_{max}. \quad (28d)$$

Problem (P3.2) is a convex optimization problem and can be addressed using convex optimization methods [9]. Next, the Lagrange duality method is employed to achieve the closed-form solutions of the CPU frequencies and the UAV's transmit power for offloading.

Proposition 2: For given WPT time allocation a and computation time t_k, the optimal solution of problem (P3.2) can be given by

$$f_k^* = \sqrt{\frac{1}{3\lambda_k \tau_k CT}}, \quad (29)$$

$$\sum_{m=k}^K P_m^* g_m = \left[\frac{Bg_k}{\lambda_k T \ln 2} - N_0\right]^+, \quad (30)$$

where $[x]^+$ indicates $\max(x, 0)$.

Proof: Please refer to Appendix A for the proof of Proposition 2. ∎

To find the optimal solution of problem (P3.2), we exploit the subgradient approach [10] where the dual variables are updated through iteration process. Therefore, in the $(n+1)$th iteration, the dual variable $\lambda_k(n+1)$ is expressed as

$$\lambda_k(n+1) = [\lambda_k(n) - \delta\Delta\lambda_k(n)]^+, \quad (34)$$

where δ denotes a sufficiently small positive step-size. $\Delta\lambda_k(n)$ is the corresponding subgradient that is given by

$$\Delta\lambda_k(n) = aT\xi_0 P_0|\mathbf{h}_k^H\mathbf{F}\mathbf{w}_k|^2 - \tau_k f_k^3 t_k - P_k(1-a)T. \quad (35)$$

For a given CPU frequency f_k^* and transmit power for offloading P_k^*, problem (P3) is reformulated as

$$(P3.3): \max_{a, t_k} \sum_{k=1}^K \left[\frac{f_k t_k}{CT}\right.$$

$$\left. + B(1-a)\log_2\left(1 + \frac{P_k g_k}{\sum_{i=k+1}^K P_i g_i + N_0}\right)\right] \quad (36a)$$

$$\text{s.t. } \tau_k f_k^3 t_k + P_k(1-a)T \le aT\xi_0 P_0|\mathbf{h}_k^H\mathbf{F}\mathbf{w}_k|^2, \quad (36b)$$

$$0 \le t_k \le T, \quad (36c)$$

$$0 \le a \le 1. \quad (36d)$$

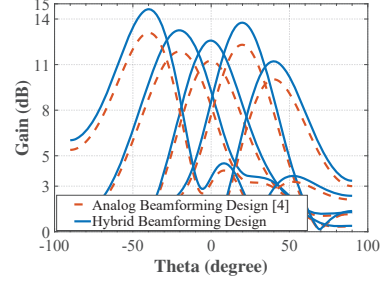**Fig. 2:** An example of the beam pattern response for the hybrid beamforming design with $\phi = 90°$.
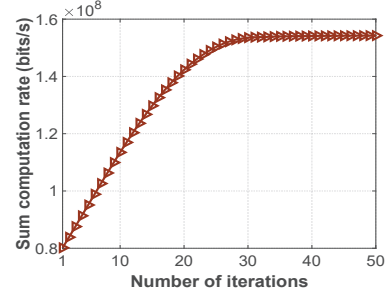

Fig. 3: An example of the convergence behavior of the resource allocation algorithm for the partial offloading mode in a multiuser UAV-aided wireless powered MEC system.

Since the objective function and constraints are linear functions with respect to a and t_k, problem (P3.3) is a linear programming problem. Thus, problem (P3.3) can be addressed effectively through the CVX toolbox.

The resource allocation algorithm for solving problem (P3) works as follows. In each iteration, (28a) is maximized over (f_k, P_k), while keeping (a, t_k)'s fixed. For a given (f_k, P_k), the set of (a, t_k) is achieved via solving problem (P3.3). The algorithm stops if it converges to a fixed point.

V. SIMULATION RESULTS

We provide numerical results to demonstrate the performance of all presented algorithms. It is assumed that the UAV-carried wireless-powered MEC network has $K = 4$ IoT devices. The 8×8 UAV-mounted antenna array is separated into four 4×4 rectangular arrays. Other parameters are as follows: $\beta_0 = -20$ dB, $\alpha = 2$, $\xi_0 = 0.8$, $P_0 = 1$ W, $B = 20$ MHz, $N_0 = 10^{-9}$ W, $C = 200$ cycles/bit, $\tau_k = 10^{-26}$, $T = 1$ s, $2\Theta = 80°$.

First, we compare the beam pattern response of our designed hybrid beamforming with that of the analog beamforming recently proposed in [4]. We assume that the excitation amplitude and element spacing of the antenna array are 1 A and 5.5 mm. As shown in Fig. 2, the main lobe responses achieved by the hybrid beamforming outperforms the analog beamforming. This is because when the analog beamforming is designed, the digital beamforming weights are optimized to further improve the gain.

In Fig. 3, we study the convergence behavior of the resource allocation algorithm for solving problem (P3). As shown in Fig. 3, since the resource allocation algorithm involves a joint WPT time allocation and computation resource scheduling procedure, the sum computation rate converges to a fixed value after around 28 iterations.

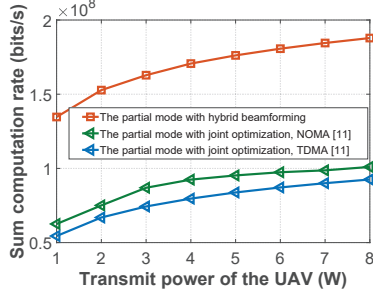In Fig. 4, we study the sum computation rate versus different

Fig. 4: The sum computation rate versus the transmit power of the UAV under the partial offloading mode.
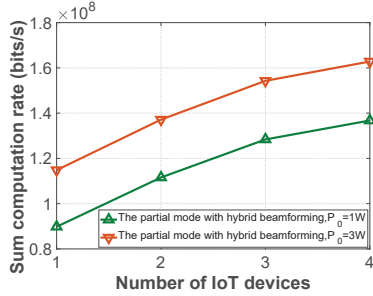

Fig. 5: The sum computation rate of all IoT devices versus the number of IoT devices under the partial offloading mode.

transmit powers. To show the computation performance, we compare with the "joint optimization" algorithm in [11]. It can be seen that the sum computation rate achieved by our resource allocation algorithm outperforms the "joint optimization" algorithm. This is due to the fact that the resource allocation algorithm enables the UAV-mounted antenna array to generate multiple beams to charge IoT devices which can compensate for the high propagation loss. Moreover, our algorithm adopts NOMA which enables multiple IoT devices to tansmit their tasks to the UAV simultaneously, and thus enhances the performance in terms of the sum computation rate [12]–[14].

Finally, we study the sum computation rate versus different number of IoT devices. In Fig. 5, the sum computation rate achieved by the resource allocation algorithm is monotonically non-decreasing with the number of IoT devices. In particular, the sum computation rate increases with a small quantity of IoT devices, i.e., $K < 3$, and then saturates when $K \geq 3$. This is because the interference is also increasing with the rising number of IoT devices, and the sum computation rate is still limited in this case.

VI. Conclusion

This paper exploited hybrid beamforming and NOMA for improving the computation performance of UAV-aided wireless-powered MEC networks. We maximized the sum computation rate at all the IoT devices via jointly optimizing the UAV's 3D position, hybrid beamforming design and computation resource allocation. To solve this problem, an effective algorithm is proposed to optimize these variables sequently. Numerical results verified that the sum computation rate of all the IoT devices can be significantly enhanced by the designed resource allocation algorithms compared to the benchmark schemes.

Appendix A
Proof Of Proposition 2

By introducing a set of non-negative dual variables, λ_k, $k = 1, \cdots, K$, associated with the energy harvesting constraints for the IoT devices in problem (P3.2), the Lagrangian function of problem (P3.2) is represented as

$$
L(\lambda_k, f_k, P_k)
$$
$$
= \sum_{k=1}^{K} \frac{f_k t_k}{C_k T} + B(1-a) \log_2 \left(\frac{\sum_{i=1}^{K} P_i g_i + N_0}{N_0} \right)
$$
$$
+ \sum_{k=1}^{K} \lambda_k \left[aT\xi_0 P_0 |\mathbf{h}_k^H \mathbf{F} \mathbf{w}_k|^2 - \tau_k f_k^3 t_k - P_k (1-a)T \right]. \quad (31)
$$

Then, the derivatives of $L(\lambda_k, f_k, P_k)$ with respect to f_k and P_k are expressed as

$$
\frac{\partial L(\lambda_k, f_k, P_k)}{\partial f_k} = \frac{t_k}{C_k T} - 3\lambda_k \tau_k f_k^2 t_k, \quad (32)
$$
$$
\frac{\partial L(\lambda_k, f_k, P_k)}{\partial P_k} = \frac{B(1-a)g_k}{\left(\sum_{m=k}^{K} P_m g_m + N_0 \right) \ln 2} - (1-a)T. \quad (33)
$$

By using the Karush-Kuhn-Tucher (KKT) conditions [9], we can obtain the optimal solutions of problem (P3.2) as (29)-(30). Therefore, this completes the proof of Proposition 2.

References

[1] W. Feng, J. Tang, Y. Yu, J. Song, N. Zhao, G. Chen, K.-K. Wong, and J. Chambers, "UAV-enabled SWIPT in IoT networks for emergency communications," *IEEE Wireless Commun.*, to be published, DOI: 10.1109/MWC.001.1900656.

[2] S. Bi and Y. J. Zhang, "Computation rate maximization for wireless powered mobile-edge computing with binary computation offloading," *IEEE Trans. Wireless Commun.*, vol. 17, no. 6, pp. 4177–4190, Jun. 2018.

[3] Z. Ding, X. Lei, G.K. Karagiannidis, R. Schober, J. Yuan, and V.K. Bhargava, "A survey on non-orthogonal multiple access for 5G networks: Research challenges and future trends," *IEEE J. Sel. Areas Commun.*, vol. 35, no. 10, pp. 2181–2195, Oct. 2017.

[4] W. Feng, N. Zhao, S. Ao, J. Tang, X. Zhang, Y. Fu, D. K. C. So, and K. K. Wong, "Joint 3D trajectory design and time allocation for UAV-enabled wireless power transfer networks," *IEEE Trans. Veh. Technol.*, vol. 69, no. 9, pp. 9265–9278, Sep. 2020.

[5] H. Tuy and F. A. Al-Khayyal, "Global optimization of a nonconvex single facility location problem by sequential unconstrained convex minimization," *J. Global Optim.*, vol. 2, no. 1, pp. 61–71, Mar. 1992.

[6] J. Borwein and A. S. Lewis, *Convex Analysis and Nonlinear Optimization: Theory and Examples*. New York, NY, USA: Springer-Verlag, 2006.

[7] C. A. Balanis, *Antenna Theory: Analysis and Design*. New York, NY, USA: Wiley, 2016.

[8] Q. Zhang and H. Li, "MOEA/D: A multi-objective evolutionary algorithm based on decomposition," *IEEE Trans. Evol. Comput.*, vol. 11, no. 6, pp. 712–731, Dec. 2007.

[9] S. Boyd and L. Vandenberghe, *Convex Optimization*. Cambridge, U.K.: Cambridge Univ. Press, 2004.

[10] D. P. Palomar and M. Chiang, "A tutorial on decomposition methods for network utility maximization," *IEEE J. Sel. Areas Commun.*, vol. 24, no. 8, pp. 1439–1451, Aug. 2006.

[11] F. Zhou, Y. Wu, R. Q. Hu, and Y. Qian, "Computation rate maximization in UAV-enabled wireless-powered mobile-edge computing systems," *IEEE J. Sel. Areas Commun.*, vol. 36, no. 9, pp. 1927–1941, Sep. 2018.

[12] F. Wang, J. Xu, and Z. Ding, "Multi-antenna NOMA for computation offloading in multiuser mobile edge computing systems," *IEEE Trans. Commun.*, vol. 67, no. 3, pp. 2450–2463, Mar. 2019.

[13] Z. Yang, C. Pan, J. Hou, and M. Shikh-Bahaei, "Efficient resource allocation for mobile-edge computing networks with NOMA: Completion time and energy minimization," *IEEE Trans. Commun.*, vol. 67, no. 11, pp. 7771–7784, Nov. 2019.

[14] Y. Ye, L. Shi, H. Sun, R. Q. Hu, and G. Lu, "System-centric computation energy efficiency for distributed NOMA-based MEC networks," *IEEE Trans. Veh. Technol.*, vol. 69, no. 8, pp. 8938–8948, Aug. 2020.